Editors' Suggestion

Polaron hopping through piecewise-linear functionals

Stefano Falletta* and Alfredo Pasquarello
Chaire de Simulation à l'Echelle Atomique (CSEA), Ecole Polytechnique Fédérale de Lausanne (EPFL), CH-1015 Lausanne, Switzerland

(Received 16 February 2023; accepted 27 April 2023; published 11 May 2023)

We use piecewise-linear functionals to study the polaron energy landscape and hopping rates in β-Ga_2O_3, which we adopt as an example of an anisotropic material hosting multiple polaronic states. We illustrate various functionals for polaron localization, including a hybrid functional and two types of semilocal functionals, and discuss how to ensure the piecewise-linearity condition. Then, we determine the formation energies of stable polarons, and show that single-site and multisite polaronic states can be found in close energetic competition. We calculate the hyperfine and superhyperfine parameters associated with each polaron, and discuss the comparison with experiment. Next, we perform nudged-elastic-band calculations to determine energy landscapes and hole transfer rates of all first-nearest-neighbor polaron hoppings. We show that when the piecewise-linearity condition is ensured polaron properties are robust upon variation of the functional adopted, including formation energies, energy barriers, and charge transfer rates. This supports the use of semilocal functionals for calculating polaron transport properties.

DOI: 10.1103/PhysRevB.107.205125

I. INTRODUCTION

Polarons are quasiparticles consisting of localized charges coupled with self-induced lattice distortions [1]. In the limit of strong electron-phonon coupling, the polaronic charge localizes over a short length scale comparable to the lattice parameter, thereby forming a small polaron. Small polarons are generally studied through first-principles methods based on density functional theory (DFT). However, standard semilocal DFT fails at describing polarons because of the spurious inclusion of the electron self-interaction [2–13]. Two descriptions of the self-interaction have been introduced: the one-body and the many-body self-interaction [2–5,7]. The one-body self-interaction refers to the charge interacting with itself, which vanishes in Hartree-Fock theory but persists in standard semilocal DFT. At variance, the many-body self-interaction is defined as the deviation from the piecewise linearity of the total energy as a function of electron occupation [2–5,7]. In this regard, it has been shown that the notion of many-body self-interaction is superior to the notion of one-body self-interaction [14,15]. Indeed, addressing the many-body self-interaction implies (i) enforcing the piecewise linearity of the total energy upon electron occupation, which is a property of the exact density functional [2], (ii) accounting for additional electron screening effects, which are overseen when correcting for the one-body self-interaction [14,15], and (iii) achieving polaron properties that are robust upon variation of the functional adopted [14–16]. Such a robustness guarantees the reliability of the theoretical predictions, particularly in the case of polarons for which experimental data are often scarce.

The many-body self-interaction of polarons is addressed when using piecewise-linear functionals. This can be achieved by adjusting parameters in hybrid functionals [11,17–34], in semilocal functionals specifically designed for polarons [14,15], or in DFT + U functionals [9,16,22,23,35–44]. The notion of piecewise linearity has already been used for studying polarons [9,19–27,34,45]. The enforcement of the piecewise linearity requires the inclusion of finite-size corrections in the energetics of polaronic defects with frozen lattice distortions [34,46], which can be achieved with model correction schemes [46]. Additionally, the recent finding that piecewise-linear functionals yield robust polaron densities, polaronic lattice bonds, and formation energies [14–16] indicates that semilocal and DFT + U functionals can be used for studying polarons. This enables efficient calculations of polarons, at a computational cost substantially lower than that of hybrid functional calculations. Moreover, it is of interest to assess whether the potential of piecewise-linear functionals extends to the study of transport properties.

Polarons have a large impact on transport properties of materials and on related applications in photovoltaics [1]. From an experimental point of view, it has been shown that small polarons follow an Arrhenius-type behavior, which is characterized by a thermally activated carrier concentration and by an increasing mobility as a function of temperature [47]. From a theoretical point of view, most of the studies on polaron hopping are based on Marcus theory [48,49] or on Emin-Holstein-Austin-Mott theory [50–52], which are equivalent for such hopping processes [53]. In these approaches, the initial and final polaron states are represented through independent Born-Oppenheimer surfaces, and a reaction pathway is defined to determine the transition state. The difference between the energies of the transition state and of the initial state gives the activation energy for the hopping process. Depending on the coupling between the initial and final states, two regimes are distinguished: for large coupling the regime is adiabatic, for small coupling the regime is diabatic [54]. Depending on the regime, different analytic expressions for the polaron hopping rate have been derived [54]. Such

*stefano.falletta@epfl.ch

expressions can be incorporated within the Landau-Zener formula [55,56], and have largely been applied to polaron hopping processes [21,53,57–71]. The theoretical framework for studying polaron hopping is thus well defined. However, in such a framework, the hopping rate depends exponentially on the activation energy, which hence needs to be accurately determined to yield reliable theoretical predictions.

The potential of piecewise-linear functionals in the determination of polaron properties can be systematically assessed when considering an anisotropic system, which can host multiple polaronic states. Indeed, the presence of various polaronic states allows for a multitude of polaron hopping pathways. This enables an extended comparison of polaron properties obtained with different piecewise-linear functionals. For this reason, as a test case, we consider monoclinic gallium oxide (β-Ga_2O_3), a promising semiconductor for power electronics and optoelectronics due to its large band gap and large breakdown field [72–77]. In particular, it has been shown that β-Ga_2O_3 can host both self-trapped holes [17,25,78–88] and impurity-trapped holes [88–100]. Hybrid functional and DFT + U calculations have shown that self-trapped holes can localize at differently coordinated oxygen sites [17,25,78–88], due to the anisotropic structure of β-Ga_2O_3. Paramagnetic resonance experiments suggest the existence of self-trapped holes at only one type of O site in β-Ga_2O_3 [92,99]. Experimental results of self-trapped holes at other O sites are missing. Additionally, previous theoretical results may also not be accurate, due to the choice of the adopted functional. For these reasons, β-Ga_2O_3 represents a prototypical material for our study.

In this work, we apply piecewise-linear hybrid and semilocal functionals to study energy landscapes and transfer rates of hole polarons in β-Ga_2O_3. We focus on this material because it can host multiple polaronic states due to its anisotropic structure. We consider the hybrid functional PBE0(α) [101], the semilocal functional introduced by Falletta and Pasquarello [14,15], and the Hubbard-corrected DFT + U functional [35–44]. We highlight that these functionals depend on one parameter, which can be tuned to enforce the piecewise-linearity condition of the total energy upon electron occupation. Using such piecewise-linear functionals, we determine the stable hole polarons, and discuss the energy competition between single-site and multisite polaronic states. We calculate the hyperfine and superhyperfine parameters associated with each polaron using the various piecewise-linear functionals, and discuss the comparison with available experimental data. Next, we calculate the energy landscape pertaining to all first-nearest-neighbor polaron hoppings through nudged-elastic-band calculations, and determine the respective hopping rates using the Marcus-Emin-Holstein-Austin-Mott theory. When ensuring the piecewise-linearity condition, we not only retrieve the robustness of ground-state polaron properties as established previously [14–16], but also find that such a robustness holds for energy barriers and hopping rates. This strongly supports the use of semilocal functionals for polaron hopping calculations.

This work is organized as follows. In Sec. II, we present the piecewise-linear functionals used in this work. In Sec. III, we determine the electronic, structural, and hyperfine properties of stable polaronic states in β-Ga_2O_3 obtained with the various piecewise-linear functionals. In Sec. IV, we determine the energy landscapes and transition rates for all first-nearest-neighbor polaron hoppings in β-Ga_2O_3. In Sec. V, we draw the conclusions.

II. PIECEWISE-LINEAR FUNCTIONALS

We illustrate various functionals that can localize polarons, namely, the hybrid functional PBE0(α) [101], the semilocal functional introduced in Refs. [14,15], which we here call γDFT, and the Hubbard-corrected DFT + U functional [35–44]. All these functionals depend on a parameter, which we denote ξ. In particular, for the PBE0(α) functional, ξ corresponds to the fraction of Fock exchange α admixed to the semilocal exchange. For the γDFT functional, ξ is the strength γ of a weak local potential dependent on the polaron density. For the DFT + U functional, ξ is the Hubbard interaction U. These functionals modify the standard semilocal Kohn-Sham equations by including an extra potential, namely,

$$\left(\mathcal{H}_\sigma^0 + V_\sigma^\xi\right)\psi_{i\sigma}^\xi = \epsilon_{i\sigma}^\xi \psi_{i\sigma}^\xi, \tag{1}$$

where $\mathcal{H}_\sigma^0$ is the semilocal Perdew-Burke-Ernzerhof (PBE) Hamiltonian [102], V_σ^ξ is the extra potential, $\psi_{i\sigma}^\xi$ are the wave functions, $\epsilon_{i\sigma}^\xi$ are the eigenvalues, and σ is the spin. For the three functionals considered, the potential V_σ^ξ takes the following expressions:

$$V_\sigma^\alpha = -\alpha V_{x\sigma} - \alpha \sum_i f_{i\sigma} \frac{|\psi_{i\sigma}^\alpha\rangle\langle\psi_{i\sigma}^\alpha|}{|\mathbf{r}-\mathbf{r}'|}, \tag{2}$$

$$V_\sigma^\gamma = q\gamma \frac{\partial V_{xc\sigma}}{\partial q}, \tag{3}$$

$$V_\sigma^U = U \sum_{Imm'} \left[\frac{\delta_{mm'}}{2} - n_{mm'}^{I\sigma}\right] |\phi_{m'}^I\rangle\langle\phi_m^I|, \tag{4}$$

where $V_{x\sigma}$ is the PBE exchange potential, $f_{i\sigma}$ is the occupation of the ith orbital in the spin channel σ, q is the polaron charge, and $\mathbf{n}^{I\sigma}$ is the occupation matrix of localized orbitals ϕ_m^I of state index m on atom I. The total energy corresponding to Eq. (1) is

$$E^\xi = E^0 + \Delta E^\xi, \tag{5}$$

where E^0 is the semilocal PBE energy, and ΔE^ξ the energy correction related to the potential V_σ^ξ. For the three functionals, the energy ΔE^ξ is given by

$$\Delta E^\alpha = -\alpha E_x[n_\uparrow^\alpha, n_\downarrow^\alpha] \tag{6}$$

$$-\frac{\alpha}{2}\sum_{ij\sigma} f_{i\sigma} f_{j\sigma} \int d\mathbf{r}\, d\mathbf{r}' \times \frac{\psi_{i\sigma}^*(\mathbf{r})\psi_{j\sigma}^*(\mathbf{r}')\psi_{j\sigma}(\mathbf{r})\psi_{i\sigma}(\mathbf{r}')}{|\mathbf{r}-\mathbf{r}'|}, \tag{7}$$

$$\Delta E^\gamma = \frac{q}{2}\sum_\sigma \int d\mathbf{r}\, V_\sigma^\gamma(\mathbf{r}) \frac{dn_\sigma^\gamma(\mathbf{r})}{dq},$$

$$\Delta E^U = \frac{U}{2}\sum_{I\sigma} \mathrm{Tr}[\mathbf{n}^{I\sigma}(1-\mathbf{n}^{I\sigma})], \tag{8}$$

where n_σ^ξ is the total electron density in the spin channel σ. The analytic expression of ΔE^γ is derived in Appendix A.

The enforcement of the piecewise-linearity condition is crucial to achieve polaron localization, which often fails when using standard semilocal functionals [14,15]. While the hybrid functional PBE0(α) gives an overall improvement of the electronic structure including band gaps and density of states [16,24,25,29,30,33,103–105], the γDFT and the DFT + U functionals specifically target the many-body self-interaction of the polaron state and are not expected to reproduce more global properties [14–16]. Indeed, the γDFT band gaps are equal to those obtained with PBE, which generally underestimate the experimental band gap. In DFT + U calculations, the U is applied to the orbitals constituting the polaron state [16], which may not be the states constituting the band edges. The piecewise linearity of the total energy as a function of the polaron occupation can be achieved by selecting $\xi = \xi_k$ such that the concavity of the total energy vanishes. Through Janak's theorem [106], this corresponds to enforcing the polaron level ϵ_p^ξ to be constant with respect to the polaron charge q, namely,

$$\frac{d^2}{dq^2}E^\xi(q)\bigg|_{\xi=\xi_k} \overset{\text{Janak}}{=} -\frac{d}{dq}\epsilon_p^\xi(q)\bigg|_{\xi=\xi_k} = 0. \tag{9}$$

For instance, in the case of a hole polaron in the spin channel $\downarrow$, Eq. (9) can be satisfied by imposing the condition $\epsilon_p^{\xi_k}(+1) = \epsilon_p^{\xi_k}(0)$, where the energy levels $\epsilon_p^{\xi_k}(+1)$ and $\epsilon_p^{\xi_k}(0)$ are calculated for the polaron structure $\mathbf{R}_{+1}^{\xi_k}$. We remark that in the enforcement of Eq. (9), the polaron level $\epsilon_p^{\gamma_k}$ could potentially resonate with the electronic bands, thus leading to charge delocalization and vanishing lattice distortions. This problem can be overcome by including a self-consistent scissor operator to the Hamiltonian, as discussed in Appendix B.

The polaron localization depends on the competition between two energy contributions: the energy gain due to charge localization and the energy cost due to lattice distortions. This can be quantified through the concept of formation energy, which is defined as [107]

$$E_f^\xi(q) = E^\xi(q) - E_{\text{ref}}^\xi(0) + q\epsilon_b^\xi, \tag{10}$$

where $E^\xi(q)$ is the total energy of the polaron system, $E_{\text{ref}}^\xi(0)$ is the total energy of the reference pristine system, and ϵ_b^ξ is the band level corresponding to the delocalized state. When the piecewise linearity is enforced [Eq. (9)], the total energy can equivalently be rewritten as

$$E^{\xi_k}(q) = E^0(0) - q\epsilon_p^{\xi_k}, \tag{11}$$

which leads to the following expression for the polaron formation energy:

$$E_f^{\xi_k}(q) = q\left(\epsilon_b^{\xi_k} - \epsilon_p^{\xi_k}\right) + \left[E^{\xi_k}(0) - E_{\text{ref}}^{\xi_k}(0)\right]. \tag{12}$$

Finite-size electrostatic corrections due to the use of periodic boundary conditions need to be applied to total energies and defect energy levels [46,107–109]. This is due to the spurious interactions of the net localized charge in the supercell with its periodic replicas and with the neutralizing background charge present in the system. In particular, in the case of polarons, one also needs to correct for the energetics of the neutral state in the presence of lattice polarization [46], which is obtained for a vanishing polaron charge in the polaronic geometry. This can be achieved by treating on an equal footing the screening of the electrons and of the ionic polarization charge arising from the lattice distortions [46]. For instance, in the case of a hole polaron, the finite-size correction for the charged ($q = +1$) and neutral ($q = 0$) energy levels in the presence of polaronic lattice distortions are given by

$$\epsilon_{\text{cor}}(+1) = -2E_m(+1, \varepsilon_0), \tag{13}$$

$$\epsilon_{\text{cor}}(0) = -2\frac{E_m(\varepsilon_\infty/\varepsilon_0 - 1, \varepsilon_\infty)}{\varepsilon_\infty/\varepsilon_0 - 1}, \tag{14}$$

where $E_m(q, \varepsilon)$ is the total energy correction for a system of charge q with screening described by the dielectric constant ε [108,109], ε_∞ the high-frequency dielectric constant, and ε_0 the static dielectric constant. The total energy of the system with a hole polaron is then corrected by $E_m(+1, \varepsilon_0)$, where the static dielectric constant ε_0 is used since both atoms and electrons are relaxed self-consistently. The code for performing these corrections is freely available [110,111]. For simplicity of notation, we consider that finite-size effects are implicitly included in the total energies and polaron levels in all formulas throughout this work. For instance, in the enforcement of Eq. (9), $\epsilon_p^{\xi_k}(q)$ is corrected as $\epsilon_p^{\xi_k}(q) + \epsilon_{\text{cor}}(q)$. Similarly, $E_f^{\xi_k}(+1)$ is corrected as $E_f^{\xi_k}(+1) + E_m(+1, \varepsilon_0)$. Without the inclusion of finite-size corrections, the polaron formation energies would be noticeably underestimated [15,16].

III. STABLE POLARONIC STATES

The calculations are performed with version 7.2 of the QUANTUM ESPRESSO suite [112], which includes the implementation of the γDFT functional and of the self-consistent scissor operator introduced in Appendix B. The core-valence interactions are described by norm-conserving pseudopotentials [113]. We model β-Ga_2O_3 with a 120-atom monoclinic supercell ($a = 12.38$Å, $b = 9.28$, $c = 11.76$Å). The energy cutoff is set to 60 Ry. The lattice parameters are determined at the PBE level of theory for the pristine system. The Brillouin zone is sampled at the Γ point. Through the application of finite electric fields [114] at the PBE level of theory, we determine the high-frequency and static dielectric constants, $\epsilon_\infty = 3.75$ and $\epsilon_0 = 11.98$, which are used for the finite-size corrections [46,108]. We remark that in β-Ga_2O_3 there are three differently coordinated O atoms. As illustrated in Fig. 1(a), we denote O_I the oxygen atom shared by two GaO_6 octahedra and one GaO_4 tetrahedron, O_{II} the oxygen atom shared by one GaO_6 octahedron and two GaO_4 tetrahedra, and O_{III} the oxygen atom coordinated with four oxygen atoms.

We investigate the stability of hole polarons in β-Ga_2O_3 using piecewise-linear PBE0(α), γDFT, and DFT + U functionals. For each polaron, we use an initial structure in which the Ga-O bonds surrounding the selected O atom have been elongated. We then perform self-consistent electronic and structural relaxations to determine the polaron structure $\mathbf{R}_{+1}^\xi$ at various values of the parameter ξ of the considered functional. For each structure, we calculate the polaron energy levels $\epsilon_p^\xi(+1)$ and $\epsilon_p^\xi(0)$, and correct for their finite-size effects through Eqs. (13) and (14), respectively. By imposing

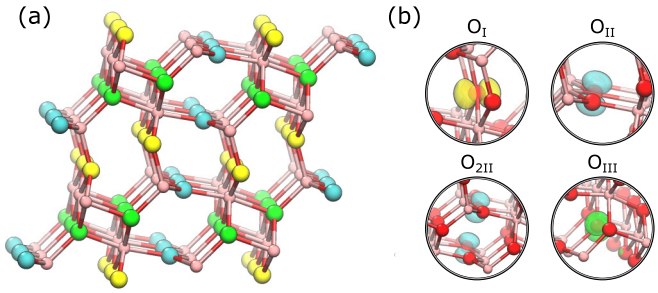

FIG. 1. (a) Bulk structure of β-Ga_2O_3 (O_I in yellow, O_{II} in cyan, O_{III} in green, Ga in pink). (b) Polaron isosurfaces at 5% of their maximum for the various hole polarons in β-Ga_2O_3 (Ga atoms in pink, O atoms in red).

$\epsilon_p^{\xi_k}(+1) = \epsilon_p^{\xi_k}(0)$ [cf. Fig. 2(a)], we find the value ξ_k that enforces the piecewise linearity of the total energy, thus suppressing the many-body self-interaction of the polaron. The polaron formation energy is then calculated with Eq. (10) with $\xi = \xi_k$. The selection of ξ_k is crucial in the determination of the polaron formation energy, in consideration of the large variations of the formation energy with ξ, as illustrated in Fig. 2(b) and as previously found in Refs. [14,15].

Using the hybrid functional PBE0(α), the enforcement of the piecewise linearity leads to hole polarons localized either at a single O_I site, at two neighboring O_{II} sites, which we denote O_{2II}, or at a single O_{III} site. For these states, we find $\alpha_k = 0.25$, 0.26, and 0.24. Considering that α_k is essentially independent of the polaronic defect, we set $\alpha_k = 0.25$ and calculate the formation energies of the three polaron states, obtaining -0.63, -0.71, and -0.39 eV, respectively.

With the semilocal functional γDFT, the enforcement of the piecewise linearity yields hole polarons localized either at a single O_I site, at a single O_{II} site, or at a single O_{III} site, with respective $\gamma_k = 1.37$, 1.45, and 1.40. Considering that γ_k is essentially independent of the polaronic defect, we take a fixed $\gamma_k = 1.4$ and find respective formation energies of -0.59, -0.56, and -0.11 eV. To avoid resonances between the polaron level and the conduction band, the conduction band manifold has been shifted by a constant amount $\Delta = 3$ eV through the use of the self-consistent scissor operator introduced in Appendix B.

In the DFT + U calculations, following Ref. [16], we apply the Hubbard U correction to the $2p$ orbitals of the O atoms,

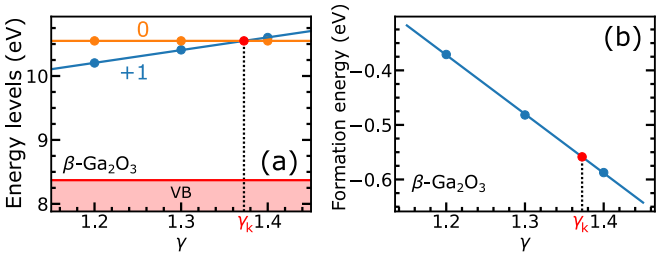

FIG. 2. (a) Energy levels and (b) formation energy obtained with γDFT as a function of γ for the hole polaron trapped at the O_I site in β-Ga_2O_3. In (a), the polaron levels are identified by their respective charge states.

TABLE I. Polaron formation energies obtained with piecewise-linear PBE0(α), γDFT, and DFT+U functionals. The formation energies of the metastable states are given in parentheses. Energies in eV.

	PBE0(α)	γDFT	DFT+U
O_I	−0.63	−0.59	−0.74
O_{II}	(−0.66)	−0.56	−0.54
O_{2II}	−0.71	(−0.25)	(−0.28)
O_{III}	−0.39	−0.11	−0.42

which constitute the localized polaron state. The enforcement of the piecewise linearity leads to polarons localized either at a single O_I site, at a single O_{II} site, or at a single O_{III} site, with respective $U_k = 4.7$, 5.1, and 4.9 eV. Considering that U_k is essentially independent of the polaronic defect, we take a fixed $U_k = 4.9$ eV and determine the respective formation energies of -0.74, -0.54, and -0.42 eV. We illustrate the various polaron states in Fig. 1(b) and give all the formation energies in Table I.

We remark that polarons localized at single O_I and O_{III} sites are achieved with all piecewise-linear functionals. However, different descriptions are found for the polaronic state involving O_{II} sites. In particular, PBE0(α) stabilizes the double-site O_{2II} state, while γDFT and DFT + U stabilize the single-site O_{II} state. The localization of hole polarons at O_I and O_{2II} sites was already reported in previous studies [17,25,83,86,88,97,99], while the localization of the hole polaron at a O_{III} site was only recently found in the work of Frodason *et al.* [86]. All such previous studies employ hybrid functionals, namely, the PBE0 functional [17,25,83,88,97,99] and a range-separated hybrid functional [86]. The adopted fraction of Fock exchange α in these works ranges from 0.26 to 0.35 [17,25,83,86,88,97,99]. For comparison, we consider the recent study of Frodason *et al.* [86], in which the O_I, O_{2II}, and O_{III} states are found. In particular, these authors calculated polaron formation energies of -0.48, -0.49, and -0.33 eV, respectively. These results systematically underestimate our PBE0(α) values in Table I, while showing similar relative stability. However, a direct comparison with all such previous studies [17,25,83,86,97,99] remains ambiguous, due to the disparity in the functional adopted and in the treatment of finite-size effects.

Our findings suggest that the hole polaron localized at a single O_{II} site is in competition with the hole polaron localized over two O_{II} sites (O_{2II}). In particular, the piecewise-linear PBE0(α) functional stabilizes the O_{2II} state, while the piecewise-linear γDFT and DFT + U functionals stabilize the O_{II} state. Here, we determine the energy of the metastable state for each functional. In the PBE0(α) calculations, we find the structure of the O_{II} state using large values of α, for which the O_{II} state is more stable than the O_{2II} state. Then, we progressively optimize the structure by lowering α to approximately α_k. Similarly, in γDFT and DFT + U calculations, we find the structures of the O_{2II} state using low values of γ and U, which we subsequently increase until approaching γ_k and U_k, respectively. As illustrated in Fig. 3, we extrapolate the formation energies of these metastable states at α_k, γ_k,

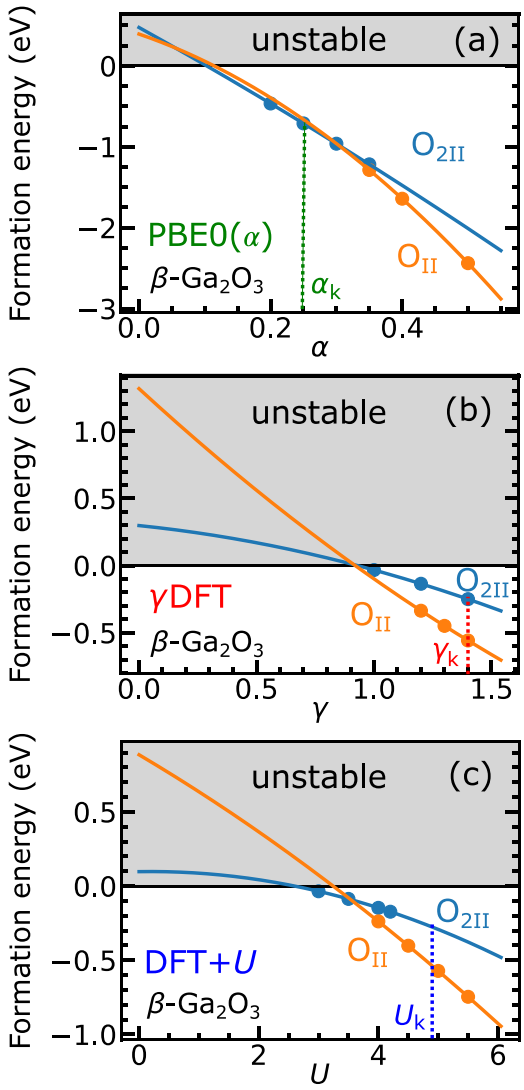

FIG. 3. Energy competition between the hole polarons localized either at the O_{II} site or at the O_{2II} site, as obtained with PBE0(α), γDFT, and DFT + U functionals.

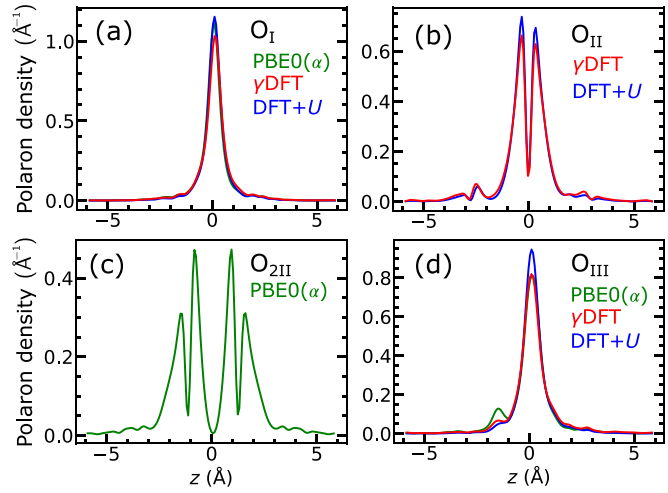

FIG. 4. Polaron densities integrated over xy planes obtained with piecewise-linear PBE0(α), γDFT, and DFT + U functionals for the hole polarons localized at the O_I, O_{II}, O_{2II}, and O_{III} sites.

and U_k, and find that for the three functionals considered the energies of the competing O_{II} and O_{2II} states lie within 0.05, 0.31, and 0.26 eV, respectively. These values are comparable with the accuracy of piecewise-linear functionals in the determination of polaron formation energies (cf. Table I). For comparison, we add to Table I the formation energies of these metastable states.

The competing O_{II} and O_{2II} states show very different polaron distributions [cf. Fig. 1(b)]. Hence, it is of interest to evaluate the parameter ξ_k' that enforces the piecewise linearity for the metastable polaronic states, namely, the O_I state in PBE0(α), the O_{2II} state in γDFT, and the O_{2II} state in DFT + U. At fixed atomic structure, the enforcement of the piecewise linearity for such states gives $\alpha_k' = 0.26$, $\gamma_k' = 2.23$, and $U_k' = 7.44$ eV. This shows that the values of α_k and α_k' obtained for the O_{2II} and O_{II} states practically coincide, in accord with previous studies showing that α_k is essentially independent of the considered defect [16,24,29,30,32]. This is due to the fact that the hybrid functional PBE0(α) addresses the self-interaction on the entire electronic manifold. At variance, the values of γ_k' and U_k' obtained for the O_{2II} state vary from the values of γ_k and U_k obtained for the O_{II} state. This can be related to the fact that γDFT and DFT + U mainly address the self-interaction of the polaron state, and hence the values of γ_k and U_k are consequently affected by the polaron distribution. Additionally, we remark that γ_k' and U_k' are both larger than γ_k and U_k, respectively. Moreover, the O_{II} state becomes more stable than the O_{2II} state for sufficiently large values of γ and U (cf. Fig. 3). This implies that self-consistent electronic and structural optimizations for the enforcement of Eq. (9) using γDFT and DFT + U functionals yield the O_{II} state. This suggests that piecewise-linear functionals may have the tendency of favoring single-site localization over multisite localization.

We now compare the properties of the stable polaronic states obtained with the various piecewise-linear functionals. As illustrated in Fig. 4, the polaron electron densities are practically independent of the adopted functional. An excellent agreement is also found for the polaronic lattice distortions, with deviations smaller than 0.05 Å (cf. Table II), with the sole exception of the weak bonds for the O_{III} state for which a deviation of 0.10 Å is observed. Similarly, differences in the formation energies due to the choice of the functional are within 0.15 eV in all cases, except for the O_{III} state where we find a larger discrepancy of 0.31 eV (cf. Table I). Overall, this analysis confirms the robustness of the polaron properties obtained with piecewise-linear functionals [14–16].

It is of interest to determine the accuracy by which γ_k, U_k, and α_k enforce the piecewise-linearity condition. This can be achieved by taking the difference between the formation energies obtained with the expressions in Eqs. (12) and (10) at $\xi = \xi_k$. Indeed, these two expressions are formally equivalent for all partial charge occupations q when the piecewise-linearity condition is satisfied. We hence determine the quantity

$$\delta = \left| E^{\xi_k}(q) - \left[E^{\xi_k}(0) - q\epsilon_p^{\xi_k} \right] \right|, \tag{15}$$

TABLE II. Lengths of Ga-O polaronic bonds (in increasing order) obtained with piecewise-linear PBE0(α), γDFT, and DFT+U functionals. The bond lengths of the metastable states are given in parentheses. Bond lengths are in Å.

	PBE0(α)	γDFT	DFT+U
O_I	1.97/2.17/2.17	2.02/2.16/2.16	1.98/2.20/2.20
O_{II}	(1.97/1.97/2.21)	2.02/2.02/2.18	1.99/1.99/2.22
O_{2II}	1.93/1.93/2.09	(1.94/1.94/2.06)	(1.93/1.93/2.08)
O_{III}	1.96/2.09/2.24/2.69	2.01/2.12/2.23/2.73	1.97/2.12/2.33/2.65

and find for the stable polarons a mean average δ of 0.02, 0.06, and 0.02 eV using γDFT, DFT + U, and PBE0(α) functionals, respectively. This agreement validates the parameters chosen to enforce the piecewise-linearity condition [cf. Eq. (9)].

We now highlight the role of the band gap in the determination of accurate polaron energetics. As illustrated in Fig. 5(a), we obtain band gaps of 4.38, 2.05, and 3.68 eV with PBE0(α_k), PBE, and DFT + U_k, respectively. The PBE0(α_k) band gap is in agreement with the range of experimental values 4.4–4.8 eV for β-Ga_2O_3 [116,117]. This is in accord with previous findings showing the accuracy of band gaps obtained with piecewise-linear hybrid functionals with respect to the experiment [11,14,15,24–30,32,33]. At variance, both PBE and DFT + U_k noticeably underestimate the experimental band gap. Nevertheless, the incorrect description of the band gap in γDFT and DFT + U is not critical for the accurate determination of polaron properties [16]. Additionally, we remark that the energy level of the hole polaron localized on a O_I site calculated with the piecewise-linear γDFT functional is in resonance with the PBE conduction band. This demonstrates the necessity of including a self-consistent scissor operator in the γDFT Hamiltonian to avoid the delocalization of the polaron wave function (cf. Appendix B).

For comparison with experiment, it is of interest to determine the hyperfine and the superhyperfine parameters of

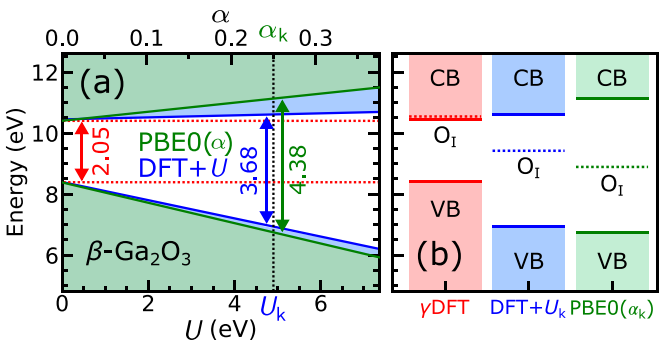

FIG. 5. (a) Band edges of β-Ga_2O_3 as obtained with PBE0(α) and DFT + U as a function of α and U, respectively. The vertical line denotes the choice of the parameter for which the piecewise-linearity condition is retrieved. The energy levels are aligned with respect to the average electrostatic potential [115]. (b) Band gaps and energy levels of the hole polaron localized at the O_I site, as obtained with γDFT, DFT + U_k, and PBE0(α_k). The γDFT band gap coincides with that obtained with PBE. The polaron level calculated with γDFT is found by applying the scissor operator to the conduction band manifold (cf. Appendix B).

O and neighboring Ga atoms, respectively, associated with each hole polaron in β-Ga_2O_3. Indeed, these parameters quantify the coupling between the unpaired electron spin and the nuclear spins, and can be measured through electron spin resonance. In particular, for each atom I, the hyperfine Hamiltonian is given by

$$\mathcal{H}_I^{\rm hyp} = \mathbf{S}_e \cdot \mathbf{A}_I \cdot \mathbf{S}_I, \tag{16}$$

where $\mathbf{A}_I$ is the hyperfine tensor, $\mathbf{S}_e$ the electronic spin, and $\mathbf{S}_I$ the nuclear spin. The components of the hyperfine tensor are given by $A_{Iij} = a_I\delta_{ij} + b_{Iij}$, where a_I is the Fermi contact interaction and b_{Iij} is a dipolar traceless term. These quantities are defined as [119]

$$a_I = \tfrac{8\pi}{3} g_e\mu_e g_I\mu_I m(\mathbf{r}_I), \tag{17}$$

$$b_{Iij} = g_e\mu_e g_I\mu_I \int d\mathbf{r}\, m(\mathbf{r}) \frac{3r_i r_j - \delta_{ij}r^2}{r^5}, \tag{18}$$

where $m = n_\uparrow - n_\downarrow$ is the spin density, g_e the electron g factor, μ_e the Bohr magneton, g_I the nuclear gyromagnetic ratio, μ_I the nuclear magneton, $\mathbf{r}_I$ the position of the ion I, and r the distance between the electron and the nucleus. The values of g_I and μ_I can be found in the literature [118]. The gyromagnetic ratio g_I is given by the ratio between the nuclear magnetic moment and the nuclear spin [119]. The eigenvalues and the associated principal directions of $\mathbf{A}_I$ can then be compared with electron paramagnetic resonance (EPR) experiments.

We perform hyperfine calculations using the GIPAW code [120,121] for all polaronic states in β-Ga_2O_3. In Table III, we give the hyperfine parameters and the corresponding principal axes for the ^{17}O atoms where polarons localize. The experimental signatures related to the ^{17}O isotope are difficult to measure because the natural abundancy of the ^{17}O isotope is less than 0.01% [99]. Thus, we also give the Fermi contact interactions obtained for Ga atoms surrounding the hole polarons in Table IV. For Ga atoms, we omit the dipolar terms, which contribute by less than 3% to the eigenvalues of the hyperfine tensor. The dipolar terms and the corresponding principal axes of ^{17}O atoms obtained with the various piecewise-linear functionals are in excellent agreement with each other. This confirms the accuracy of the spin densities, in accord with our previous findings on the polaron density (cf. Fig. 4). The Fermi contact interactions of ^{69}Ga isotopes obtained with the various piecewise-linear functionals are also in good agreement with each other. Larger discrepancies are found for the Fermi contact interactions of ^{17}O atoms. In this case, the O $2p$ orbitals that constitute the polaron wave function do not contribute [cf. Eq. (17)], and the discrepancy can be related to the description of the s orbitals of the O atom

TABLE III. Eigenvalues A_η of the hyperfine tensor and spherical angles (θ_η, ϕ_η) of the corresponding principal directions for ^{17}O atoms hosting a hole polaron in β-Ga_2O_3 ($\eta = x, y, z$). Hyperfine parameters are given in Gauss. In the case of the hole polaron localized at the O_{2II} site, the results for the two O sites where the polaron localizes are averaged with the exception of the angle θ_x, which assumes two distinct values for the two O_{II} sites involved.

	O_I			O_{II}			O_{2II}			O_{III}		
	PBE0(α_k)	γDFT	DFT+U_k	PBE0(α_k)	γDFT	DFT+U_k	PBE0(α_k)	γDFT	DFT+U_k	PBE0(α_k)	γDFT	DFT+U_k
a	−29	−82	−27	−30	−76	−28	−31	−51	−20	−27	−76	−26
b_x	49	52	51	44	52	51	29	31	29	45	51	50
b_y	49	53	52	44	51	51	29	31	29	45	52	51
b_z	−98	−105	−103	−88	−103	−102	−58	−62	−58	−90	−103	−101
A_x	20	−30	24	14	−24	23	−2	−20	9	18	−25	24
A_y	20	−29	25	14	−25	23	−2	−20	9	18	−24	25
A_z	−127	−187	−130	−118	−179	−130	−89	−113	−78	−117	−179	−127
θ_x	3°	2°	4°	90°	90°	90°	76°/104°	76°/104°	77°/104°	129°	126°	122°
ϕ_x	−1°	4°	−1°	89°	90°	90°	0°	0°	0°	10°	10°	4°
θ_y	90°	90°	90°	75°	105°	106°	90°	90°	90°	55°	131°	138°
ϕ_y	90°	90°	90°	−1°	0°	0°	90°	90°	90°	135°	141°	138°
θ_z	93°	92°	94°	16°	15°	16°	14°	14°	13°	121°	117°	114°
ϕ_z	0°	0°	0°	0°	0°	0°	0°	0°	0°	70°	78°	78°

at which the polaron localizes. The Fermi contact interactions obtained with PBE0(α_k) and DFT + U_k are found to be very close. However, it remains to be ascertained whether this accord carries broader validity beyond the specific case of β-Ga_2O_3. The superhyperfine parameters of Ga atoms neighboring the hole polarons localized at the O_I and O_{2II} sites have also been calculated by Skachkov *et al.* [99]. In particular, these authors used the DFT + U functional with $U = 4$ eV and found $a = -16, -8$, and -8 G for the O_I state and $a = -13, -12$, and -9 G for the O_{2II} state, which are lower than our values. The differences are due to the dependence of the Fermi contact interaction on the value of the spin density at the ion site [cf. Eq. (17)], which is sensitive to the details of the electronic structure, as previously observed by Skachkov *et al.* [99]. A quantitative comparison with experimental values might also require the inclusion of dynamical Jahn-Teller and spin-orbit coupling effects [99].

In relation to a specific EPR signal, Kananen *et al.* suggested that the hole polaron localized at the O_I site could be compatible with the experiment [82]. This is based on a geometric analysis relating the orientation of the polaron density and the measured **g** tensor [82]. Moreover, for interpreting the observed EPR signal, Kananen *et al.* assumed that the hyperfine interaction with the two neighboring sixfold-coordinated Ga atoms would be much larger than with the more distant fourfold-coordinated Ga neighbor. However, in a subsequent study, Skatchkov *et al.* found that the hyperfine coupling is sizable for all three Ga neighbors, and that the largest interaction is actually found for the fourfold-coordinated Ga neighbor [99], in contrast with the assumptions of Kananen *et al.* Thus, Skatchkov *et al.* inferred that hole polarons are not at the origin of the EPR data [99]. Our calculated Fermi contact interactions are also sizable for more than two Ga atoms, and their relative magnitude is in agreement with the results of Skatchkov *et al.* Hence, our results also suggest that the EPR signal first observed by Kananen *et al.* unlikely results from localized hole polarons. The difficulty in measuring polaron-related signals likely results from the n-type character of β-Ga_2O_3 samples, which favors rapid hole polaron annihilation by electron-hole recombination [82].

IV. POLARON HOPPING

The energy landscape of a polaron hopping process can be determined using nudged-elastic-band (NEB) calculations [122], which allow one to determine the minimal energy path connecting initial and final states. This is achieved by discretizing the path in a series of images, and by minimizing

TABLE IV. Fermi contact interaction of ^{69}Ga atoms surrounding the hole polarons in β-Ga_2O_3. We consider ^{69}Ga isotopes, which are 60.1% abundant [99]. The values for ^{71}Ga isotopes (39.9% abundant [99]) can be achieved by multiplying those for ^{69}Ga isotopes by 1.27059 [118]. Ga(I) denotes a fourfold-coordinated Ga atom, while Ga(II) denotes a sixfold-coordinated Ga atom. Values are given in Gauss. For the hole polaron localized at the O_{2II} site, the values given correspond to an average over the two O sites.

	O_I			O_{II}			O_{2II}			O_{III}		
	PBE0(α_k)	γDFT	DFT+U_k	PBE0(α_k)	γDFT	DFT+U_k	PBE0(α_k)	γDFT	DFT+U_k	PBE0(α_k)	γDFT	DFT+U_k
Ga(I)	−35	−43	−29	−27	−32	−22	−24	−36	−24	−34	−43	−28
Ga(I)				−27	−32	−22	−24	−36	−24	−31	−40	−27
Ga(II)	−16	−28	−12	−13	−19	−10	−17	−27	−17	−22	−25	−22
Ga(II)	−16	−28	−12							−11	−9	−11

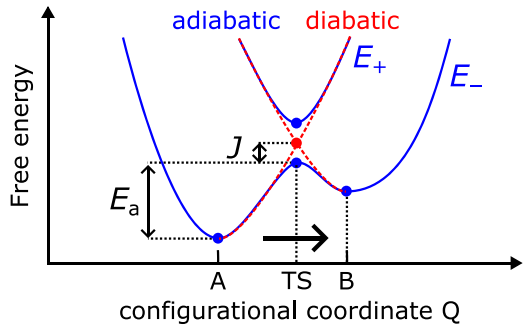

FIG. 6. Energy profile for electron transfer from the initial state A to the final state B along a configurational coordinate Q. The activation energy E_a, the coupling J between the two states, the lower and upper adiabatic energy surfaces E_- and E_+, and the transition state (TS) are indicated.

the forces orthogonal to the path for all intermediate images [122]. The energy landscape is then projected along a configurational coordinate Q. A common choice for Q is

$$(Q^n)^2 = \sum_I m_I \left|\mathbf{r}_I^n - \mathbf{r}_I^1\right|^2, \tag{19}$$

where n is the image index, m_I the mass of atom I, and $\mathbf{r}_I^n$ the Cartesian coordinate of atom I in the nth image. Once the energy profile along the configurational coordinate Q is obtained, the rate of polaron charge transfer from the initial to the final state can be calculated using the Marcus-Emin-Holstein-Austin-Mott theory [48–52]. Depending on the coupling between the initial and final states, two regimes can be distinguished [57]. For small coupling, the regime is diabatic and the energy of the transition state is found in correspondence of the intersection of the Born-Oppenheimer surfaces of the initial and final states. For large coupling, the regime is adiabatic and the transition state is more stable than the one obtained in the diabatic case. A schematical illustration of the energy profiles in these two regimes is given in Fig. 6.

Then, the charge transfer rate k_t for the hopping from an initial state to a final state can be calculated using the Landau-Zener formula [54–57], namely,

$$k_t = \kappa \nu \Gamma \exp\left(-\frac{E_a}{k_B T}\right), \tag{20}$$

where κ is the thermally averaged electronic transmission coefficient, ν an effective nuclear frequency along the reaction coordinate, Γ the nuclear tunneling factor, E_a the activation energy, and T the temperature. The tunneling factor Γ takes into account the nuclear quantum effects and can generally be approximated as $\Gamma \approx 1$, except when considering low temperatures or light elements [67]. The effective nuclear frequency ν can be calculated as [21]

$$\nu^2 = \frac{\partial^2 E(Q)}{\partial Q^2}, \tag{21}$$

and can be estimated from the NEB energy profile around the initial state within an effective one-dimensional phonon frequency approximation [123,124]. We remark that presence of the atomic masses in Eq. (19) allows one to directly associate the right-hand side of Eq. (21) to the nuclear frequency ν. The transmission coefficient κ describes the transition probability from the initial state to the final state through multiple passages via the intersection point between the diabatic surfaces [54–57]. By denoting $(1-P)$ the probability of the diabatic transition at the transition state from the low-energy adiabatic surface to the high-energy adiabatic surface and vice versa (cf. Fig. 6), κ can be expressed as [54–57]

$$\kappa = P + (1-P)^2 \sum_{k=0}^{\infty} P^{2k+1} = \frac{2P}{1+P}, \tag{22}$$

where it is assumed that no transition occurs when the system falls back to the initial state [54]. The probability P is calculated as [54–57]

$$P = 1 - \exp\left[-\frac{\pi^2 J^2}{h\nu\sqrt{4\pi (E_a + J) k_B T}}\right], \tag{23}$$

where h is the Planck constant, k_B the Boltzmann constant, and J the coupling between initial and final states (cf. Fig. 6). We note that $E_a + J$ corresponds to the diabatic activation energy, as schematically illustrated in Fig. 6. The coupling J can be calculated as the difference of the bonding and antibonding energy levels at the transition state [125]. For $P \to 1$ the regime is adiabatic, whereas the regime is diabatic for $P \to 0$.

We now study the minimal energy path for hopping of hole polarons in β-Ga_2O_3 by performing NEB calculations with piecewise-linear γDFT and DFT + U functionals. We avoid the use of the hybrid functional PBE0(α) for NEB calculations, which would require an excessively large amount of computational resources. We consider all the 21 first-nearest-neighbor hoppings, which are indexed in Table V by the pairs of O sites involved in the hopping and their respective distance. This requires performing 14 NEB calculations with each functional since hoppings involving two different O sites provide information on both forward and backward transitions. In particular, for each NEB we take a 15-image path connecting the initial and final states. We use a fixed ξ_k instead of an image-dependent one, as this affects the activation energies in a minor fashion [16]. In this way, we determine the energy landscape as a function of the reaction coordinate Q.

For each transition, we determine the activation energy E_a as the difference between the transition-state energy and the ground-state energy of the initial state. For illustration, we show in Fig. 7 the hopping process between two O_I sites connected through a Ga atom. In this case, we find very good agreement between the activation energies obtained with piecewise-linear γDFT and DFT + U functionals, obtaining barriers of 0.41 and 0.47 eV, respectively. In particular, the activation energies in the two cases differ by only 58 meV. These results are also in good agreement with the value of 0.40 eV found by Varley *et al.* for the same hopping process [17]. In Fig. 7, we also give the energy barriers calculated with the piecewise-linear PBE0(α) functional for the NEB pathways obtained with γDFT and DFT + U, finding a negligible difference of 7 meV between the two paths. This further corroborates the reliability of piecewise functionals and their mutual equivalence.

TABLE V. Distance d between hopping sites (in Å), activation energy E_a (in meV), effective nuclear frequencies $h\nu$ (in meV), and hole transfer rate k_t (in Hz) at 300 K for all first-nearest-neighbor polaron hoppings in β-Ga_2O_3, as obtained with piecewise-linear γDFT and DFT+U functionals.

		γDFT					DFT+U				
Hopping	Index	d	E_a	$h\nu$	J	k_t	d	E_a	$h\nu$	J	k_t
$O_I \rightarrow O_I$	1	3.16	674	74	198	8.4×10^{1}	3.28	653	119	260	3.1×10^{2}
	2	3.09	408	113	647	3.8×10^{6}	3.09	466	118	696	4.3×10^{5}
$O_I \rightarrow O_{II}$	3	2.88	404	77	607	3.0×10^{6}	2.83	560	124	676	1.2×10^{4}
	4	2.98	673	45	171	7.6×10^{1}	2.94	734	106	302	1.2×10^{1}
$O_I \rightarrow O_{III}$	5	2.65	693	74	602	4.2×10^{1}	2.67	647	82	680	2.6×10^{2}
	6	2.88	677	77	645	7.9×10^{1}	2.90	554	271	790	3.2×10^{4}
	7	3.24	720	99	564	1.9×10^{1}	3.23	692	97	623	5.7×10^{1}
$O_{II} \rightarrow O_I$	8	2.88	375	123	607	1.5×10^{7}	2.83	372	168	676	2.3×10^{7}
	9	2.98	642	136	171	5.4×10^{2}	2.94	547	174	302	2.7×10^{4}
$O_{II} \rightarrow O_{II}$	10	3.04	467	106	344	3.7×10^{5}	3.06	477	168	350	4.0×10^{5}
	11	3.09	416	109	443	2.7×10^{6}	3.09	441	164	490	1.6×10^{6}
	12	2.84	326	59	547	4.7×10^{7}	2.82	267	146	725	1.2×10^{9}
$O_{II} \rightarrow O_{III}$	13	2.94	703	90	479	3.3×10^{1}	2.96	744	86	144	6.7×10^{0}
	14	2.99	637	96	589	4.6×10^{2}	2.98	524	147	567	5.7×10^{4}
$O_{III} \rightarrow O_I$	15	2.65	214	73	602	4.5×10^{9}	2.67	334	140	680	8.4×10^{7}
	16	2.88	205	129	645	1.1×10^{10}	2.90	241	31	790	6.7×10^{8}
	17	3.24	246	106	564	1.9×10^{9}	3.23	369	146	623	2.2×10^{7}
$O_{III} \rightarrow O_{II}$	18	2.94	251	76	479	1.1×10^{9}	2.96	617	165	144	1.6×10^{3}
	19	2.99	179	61	589	1.5×10^{10}	2.98	398	103	567	5.2×10^{6}
$O_{III} \rightarrow O_{III}$	20	2.69	497	77	428	8.3×10^{4}	2.70	427	106	610	1.7×10^{6}
	21	3.09	511	76	349	4.9×10^{4}	3.09	491	65	489	9.0×10^{4}

When considering all other hopping processes, we find overall a similar good agreement between the activation energies obtained with γDFT and DFT + U, as given in Table I. In particular, the mean absolute error of activation energies amounts to only 85 meV [cf. Fig. 8(a)]. The largest variations are observed for the transitions $O_{III} \rightarrow O_{II}$ (indices No. 18 and No. 19), which can be related to the discrepancy in the energy difference between final and initial states involved in the NEB calculation (cf. Table I). This can be related to the Bell-Evans-Polanyi principle, which establishes a linear relationship between the activation energy and the energy difference between final and initial states [126,127].

Then, we focus on the determination of the hole transfer rates for all transitions. First, we calculate the effective nuclear frequency ν through quadratic interpolation of the energy profile around the initial state, as shown in Fig. 7. Then, we determine the couplings J for all transitions as half the separation between occupied and unoccupied defect energy levels at the transition state [125], as illustrated in Fig. 9. Given the activation energies E_a, the effective nuclear frequencies ν, and the couplings J, we calculate the probabilities P defined in Eq. (23) at $T = 300$ K. We find that $P = 1$ in all cases, with the exception of the transition No. 18 calculated with DFT +

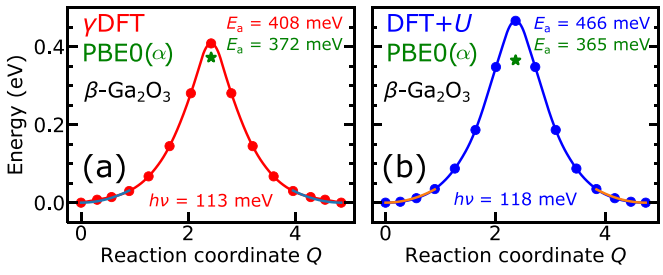

FIG. 7. Energy landscape of a polaron hopping between two neighboring O_I sites connected through a Ga atom in β-Ga_2O_3 (transition index No. 2 in Table V), as obtained with piecewise-linear (a) γDFT and (b) DFT + U functionals through the NEB method. The activation energies E_a and the effective nuclear frequencies ν are indicated. In green, we give the activation energies calculated with the piecewise-linear functional PBE0(α) for the same NEB pathway.

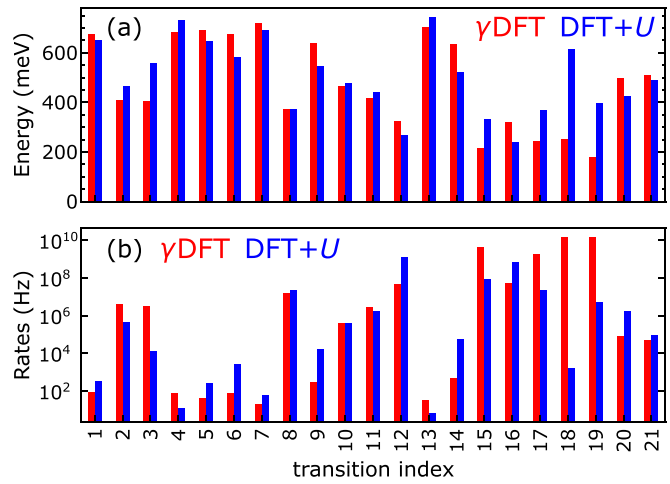

FIG. 8. (a) Activation energies and (b) hole transfer rates at 300 K for the hole polaron hoppings in β-Ga_2O_3 listed in Table V.

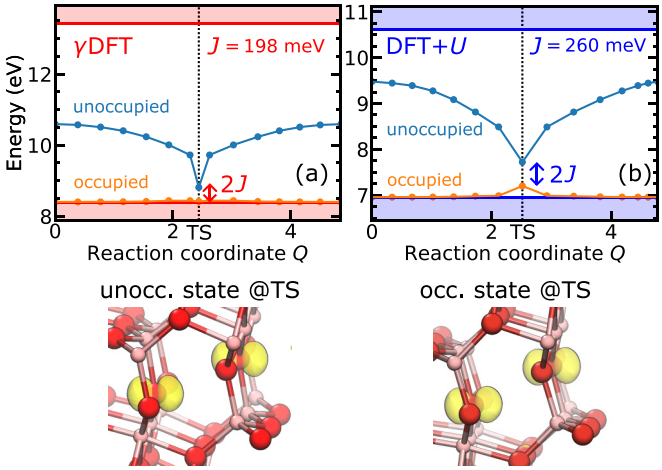

FIG. 9. Occupied and unoccupied defect energy levels as a function of the reaction coordinate for a polaron hopping between two neighboring O_I sites in β-Ga_2O_3 (transition index No. 1 in Table V), as obtained with piecewise-linear (a) γDFT and (b) DFT + U functionals. Defect energy levels are corrected by finite-size effects. Below, isodensity surfaces at 5% of their maximum for the densities of the occupied and unoccupied defect states at the transition state, as calculated with γDFT.

U for which $P = 0.9$. This indicates that essentially all the transitions are adiabatic. We then calculate the hole transfer rates at $T = 300$ K for all hopping processes using Eq. (20). The effective nuclear frequencies ν, the couplings J, and the rates k_t obtained for all the hoppings are given in Table V.

As shown in Fig. 8(b), we also find good agreement for the hole transfer rates calculated with γDFT and DFT + U, characterized by a mean value of $|\log_{10}(k_t^{\gamma_k}/k_t^{U_k})|$ equal to 1.5, which represents the mean absolute error on the order of magnitude of k_t. This is quite satisfactory considering that even small variations of the activation energy can affect the hole transfer rate by several orders of magnitude due to the exponential dependence of the transfer rate on the activation energy [cf. Eq. (20)]. This analysis sets the overall accuracy of piecewise-linear functionals in the determination of electron transfer rates, and shows that the robustness of the polaron properties obtained with piecewise-linear functionals also holds for activation energies and hopping rates.

We remark that some of the activation barriers in Table V are higher than the formation energies of the initial state. In such a case, the transition state is less stable than the delocalized state in which the polaron charge delocalizes uniformly over the entire system and the polaronic lattice distortions vanish. This indicates that the hole polaron diffusion in β-Ga_2O_3 cannot be uniquely described by polaron hopping, and that more complex scattering mechanisms combining polaron hopping and polaron delocalization should be considered in the calculation of polaron mobilities.

V. CONCLUSIONS

In conclusion, we investigated the use of piecewise-linear functionals for the determination of polaronic ground-state and transport properties. We showed that enforcing the piecewise-linearity condition leads to robust polaron properties upon variation of the functional. Considered properties include electron densities, lattice bonds, formation energies, hyperfine and superhyperfine parameters, activation energies, and transfer rates. Such a robustness validates the accuracy and the reliability of the calculated polaron properties. This is particularly relevant when considering formation energies, which are subject to large variations upon varying the parameters of the functionals.

By consequence, our work demonstrates that semilocal functionals yield essentially the same polaron properties, thereby supporting their use for exploring polaronic energy landscapes and for determining polaron transport properties. This becomes important when considering anisotropic materials, which can be characterized by numerous polaronic hopping pathways for which hybrid-functional calculations would be computationally beyond reach.

In summary, our work provides a paradigm shift for the study of polaron transport properties, through the use of piecewise-linear functionals as opposed to standard functionals. This also lends justification to the use of efficient semilocal functionals, thus paving the way to accurate and systematic studies of polaronic transport properties from first principles.

Material associated to this work can be found on Materials Cloud [128].

ACKNOWLEDGMENTS

We thank K. Bevan and Y. Ping for relevant insight, and G. Palermo and J. Lan for fruitful discussions. The calculations have been performed at the Swiss National Supercomputing Centre (CSCS) (grant under Project ID No. s1122) and at SCITAS-EPFL.

APPENDIX A: γDFT ENERGY FUNCTIONAL

In this Appendix, we derive the expression of the total energy ΔE^γ in Eq. (7). We assume that the total energy is well described by an expansion up to second order in q [14,15]. Then, ΔE^γ can be written as

$$\Delta E^\gamma(q) = \Delta E^\gamma(0) + q\left.\frac{d\Delta E^\gamma}{dq}\right|_{q=0} + \frac{q^2}{2}\frac{d^2(\Delta E^\gamma)}{dq^2}. \quad \text{(A1)}$$

We remark that $\Delta E^\gamma(0) = 0$ since the potential V_σ^γ vanishes at $q = 0$. Moreover, since V_σ^γ is linear in q then also $d(\Delta E^\gamma)/dq$ is linear in q, which thus vanishes at $q = 0$. Hence, by using the chain rule for derivatives with respect to q, Eq. (A1) can be rewritten as

$$\Delta E^\gamma(q) = \frac{q^2}{2}\sum_{\sigma\sigma'}\int d\mathbf{r}\, d\mathbf{r}'\, \frac{\delta^2(\Delta E^\gamma)}{\delta n_\sigma^\gamma(\mathbf{r})\delta n_{\sigma'}^\gamma(\mathbf{r}')}\frac{dn_\sigma^\gamma(\mathbf{r})}{dq}\frac{dn_{\sigma'}^\gamma(\mathbf{r}')}{dq}. \quad \text{(A2)}$$

Similarly, the potential V_σ^γ in Eq. (3) can be expanded in q as follows:

$$V_\sigma^\gamma(\mathbf{r}) = q\sum_{\sigma'}\int d\mathbf{r}'\, \frac{\delta V_\sigma^\gamma(\mathbf{r})}{\delta n_{\sigma'}^\gamma(\mathbf{r}')}\frac{dn_{\sigma'}^\gamma(\mathbf{r}')}{dq}. \quad \text{(A3)}$$

Using the variational relation $V_\sigma^\gamma(\mathbf{r}) = \delta(\Delta E^\gamma)/\delta n_\sigma^\gamma(\mathbf{r})$ in Eq. (A3), and inserting the resulting expression in Eq. (A2),

we obtain

$$\Delta E^{\gamma}(q) = \frac{q}{2}\sum_{\sigma}\int d\mathbf{r}\, V_{\sigma}^{\gamma}(\mathbf{r})\frac{dn_{\sigma}^{\gamma}(\mathbf{r})}{dq}, \tag{A4}$$

which can be evaluated by finite differences as

$$\Delta E^{\gamma}(q) = \frac{1}{2}\sum_{\sigma}\int d\mathbf{r}\, V_{\sigma}^{\gamma}(\mathbf{r})\left[n_{\sigma}^{\gamma}(q,\mathbf{r}) - n_{\sigma}^{\gamma}(0,\mathbf{r})\right]. \tag{A5}$$

The expression in Eq. (A5) is valid for any potential V_{σ}^{γ} with a prefactor q in V_{σ}^{γ}, under the assumption of quadraticity of the total energy with q.

APPENDIX B: SELF-CONSISTENT SCISSOR OPERATOR

In this Appendix, we discuss the self-consistent scissor operator used for opening the band gap. We remark that, in the case of electron polarons, the polaron level is stabilized by going down in energy with respect to the conduction band. At variance, in the case of hole polarons, the polaron level is stabilized by going up in energy with respect to the valence band. Considering that in semilocal density functional theory the band gap is underestimated, resonances involving the electron (hole) polaron state with the valence (conduction) band states could occur, which may prevent polaron localization.

This problem can be overcome by including in the Hamiltonian a scissor operator $\mathcal{S}_{\sigma}$ that artificially increases the band gap of the system. The scissor operator only affects electron bands that are unrelated to the polaronic state. This allows one to address resonances between the polaron level and the delocalized band states, without affecting the polaron properties. The adopted scissor operator has the expression

$$\mathcal{S}_{\sigma} = \Delta \sum_{i\in\mathcal{M}_{\sigma}^{\xi}} \left|\psi_{i\sigma}^{\xi}\right\rangle\left\langle\psi_{i\sigma}^{\xi}\right|, \tag{B1}$$

where $\psi_{i\sigma}^{\xi}$ are the wave functions obtained in the self-consistent optimization of the Kohn-Sham equations, and Δ is a constant. For electron polarons, $\mathcal{M}_{\sigma}^{\xi}$ denotes the manifold of valence-band states and Δ is taken to be negative, while for hole polarons $\mathcal{M}_{\sigma}^{\xi}$ denotes the manifold of conduction-band states and Δ is taken to be positive. The energy levels of all states belonging to the manifold $\mathcal{M}_{\sigma}^{\xi}$ are then shifted by the amount Δ. When $\mathcal{M}_{\sigma}^{\xi}$ denotes the valence-band manifold, the inclusion of $\mathcal{S}_{\sigma}$ in the Hamiltonian shifts the total energy by a contribution $N\Delta$, where N is the number of valence electrons.

[1] C. Franchini, M. Reticcioli, M. Setvin, and U. Diebold, Polarons in materials, Nat. Rev. Mater. **6**, 560 (2021).

[2] J. P. Perdew, R. G. Parr, M. Levy, and J. L. Balduz, Density-Functional Theory for Fractional Particle Number: Derivative Discontinuities of the Energy, Phys. Rev. Lett. **49**, 1691 (1982).

[3] A. Ruzsinszky, J. P. Perdew, G. I. Csonka, O. A. Vydrov, and G. E. Scuseria, Density functionals that are one- and two- are not always many-electron self-interaction-free, as shown for H_2^+, He_2^+, LiH^+, and Ne_2^+, J. Chem. Phys. **126**, 104102 (2007).

[4] Y. Zhang and W. Yang, A challenge for density functionals: Self-interaction error increases for systems with a noninteger number of electrons, J. Chem. Phys. **109**, 2604 (1998).

[5] W. Yang, Y. Zhang, and P. W. Ayers, Degenerate Ground States and a Fractional Number of Electrons in Density and Reduced Density Matrix Functional Theory, Phys. Rev. Lett. **84**, 5172 (2000).

[6] T. Schmidt and S. Kümmel, One- and many-electron self-interaction error in local and global hybrid functionals, Phys. Rev. B **93**, 165120 (2016).

[7] P. Mori-Sánchez, A. J. Cohen, and W. Yang, Many-electron self-interaction error in approximate density functionals, J. Chem. Phys. **125**, 201102 (2006).

[8] A. J. Cohen, P. Mori-Sánchez, and W. Yang, Insights into current limitations of density functional theory, Science **321**, 792 (2008).

[9] S. Lany and A. Zunger, Polaronic hole localization and multiple hole binding of acceptors in oxide wide-gap semiconductors, Phys. Rev. B **80**, 085202 (2009).

[10] A. Ruzsinszky, J. P. Perdew, G. I. Csonka, O. A. Vydrov, and G. E. Scuseria, Spurious fractional charge on dissociated atoms: Pervasive and resilient self-interaction error of common density functionals, J. Chem. Phys. **125**, 194112 (2006).

[11] L. Kronik and S. Kümmel, Piecewise linearity, freedom from self-interaction, and a Coulomb asymptotic potential: three related yet inequivalent properties of the exact density functional, Phys. Chem. Chem. Phys. **22**, 16467 (2020).

[12] V. Atalla, I. Y. Zhang, O. T. Hofmann, X. Ren, P. Rinke, and M. Scheffler, Enforcing the linear behavior of the total energy with hybrid functionals: Implications for charge transfer, interaction energies, and the random-phase approximation, Phys. Rev. B **94**, 035140 (2016).

[13] T. Körzdörfer, S. Kümmel, and M. Mundt, Self-interaction correction and the optimized effective potential, J. Chem. Phys. **129**, 014110 (2008).

[14] S. Falletta and A. Pasquarello, Many-Body Self-Interaction and Polarons, Phys. Rev. Lett. **129**, 126401 (2022).

[15] S. Falletta and A. Pasquarello, Polarons free from many-body self-interaction in density functional theory, Phys. Rev. B **106**, 125119 (2022).

[16] S. Falletta and A. Pasquarello, Hubbard U through polaronic defect states, npj Comput. Mater. **8**, 263 (2022).

[17] J. B. Varley, A. Janotti, C. Franchini, and C. G. Van de Walle, Role of self-trapping in luminescence and p-type conductivity of wide-band-gap oxides, Phys. Rev. B **85**, 081109(R) (2012).

[18] A. R. Elmaslmane, J. Wetherell, M. J. P. Hodgson, K. P. McKenna, and R. W. Godby, Accuracy of electron densities obtained via Koopmans-compliant hybrid functionals, Phys. Rev. Mater. **2**, 040801(R) (2018).

[19] J. J. Carey and K. P. McKenna, Screening doping strategies to mitigate electron trapping at anatase TiO_2 surfaces, J. Phys. Chem. C **123**, 22358 (2019).

[20] J. A. Quirk, V. K. Lazarov, and K. P. McKenna, First-principles modeling of oxygen-deficient anatase TiO_2 nanoparticles, J. Phys. Chem. C **124**, 23637 (2020).

[21] J. J. Carey, J. A. Quirk, and K. P. McKenna, Hole polaron migration in bulk phases of TiO_2 using hybrid density functional theory, J. Phys. Chem. C **125**, 12441 (2021).

[22] J. J. Carey and K. P. McKenna, Does polaronic self-trapping occur at anatase TiO_2 surfaces? J. Phys. Chem. C **122**, 27540 (2018).

[23] A. R. Elmaslmane, M. B. Watkins, and K. P. McKenna, First-principles modeling of polaron formation in TiO_2 polymorphs, J. Chem. Theory Comput. **14**, 3740 (2018).

[24] G. Miceli, W. Chen, I. Reshetnyak, and A. Pasquarello, Nonempirical hybrid functionals for band gaps and polaronic distortions in solids, Phys. Rev. B **97**, 121112(R) (2018).

[25] P. Deák, Q. Duy Ho, F. Seemann, B. Aradi, M. Lorke, and T. Frauenheim, Choosing the correct hybrid for defect calculations: A case study on intrinsic carrier trapping in β-Ga_2O_3, Phys. Rev. B **95**, 075208 (2017).

[26] B. Sadigh, P. Erhart, and D. Åberg, Variational polaron self-interaction-corrected total-energy functional for charge excitations in insulators, Phys. Rev. B **92**, 075202 (2015).

[27] N. Sai, P. F. Barbara, and K. Leung, Hole Localization in Molecular Crystals from Hybrid Density Functional Theory, Phys. Rev. Lett. **106**, 226403 (2011).

[28] S. Refaely-Abramson, S. Sharifzadeh, M. Jain, R. Baer, J. B. Neaton, and L. Kronik, Gap renormalization of molecular crystals from density-functional theory, Phys. Rev. B **88**, 081204(R) (2013).

[29] T. Bischoff, J. Wiktor, W. Chen, and A. Pasquarello, Nonempirical hybrid functionals for band gaps of inorganic metal-halide perovskites, Phys. Rev. Mater. **3**, 123802 (2019).

[30] T. Bischoff, I. Reshetnyak, and A. Pasquarello, Adjustable potential probes for band-gap predictions of extended systems through nonempirical hybrid functionals, Phys. Rev. B **99**, 201114(R) (2019).

[31] N. Österbacka, P. Erhart, S. Falletta, A. Pasquarello, and J. Wiktor, Small electron polarons in $CsPbBr_3$: Competition between electron localization and delocalization, Chem. Mater. **32**, 8393 (2020).

[32] T. Bischoff, I. Reshetnyak, and A. Pasquarello, Band gaps of liquid water and hexagonal ice through advanced electronic-structure calculations, Phys. Rev. Res. **3**, 023182 (2021).

[33] J. Yang, S. Falletta, and A. Pasquarello, One-shot approach for enforcing piecewise linearity on hybrid functionals: Application to band gap predictions, J. Phys. Chem. Lett. **13**, 3066 (2022).

[34] S. Kokott, S. V. Levchenko, P. Rinke, and M. Scheffler, First-principles supercell calculations of small polarons with proper account for long-range polarization effects, New J. Phys. **20**, 033023 (2018).

[35] V. I. Anisimov and O. Gunnarsson, Density-functional calculation of effective Coulomb interactions in metals, Phys. Rev. B **43**, 7570 (1991).

[36] V. I. Anisimov, J. Zaanen, and O. K. Andersen, Band theory and Mott insulators: Hubbard U instead of stoner I, Phys. Rev. B **44**, 943 (1991).

[37] V. I. Anisimov, I. V. Solovyev, M. A. Korotin, M. T. Czyżyk, and G. A. Sawatzky, Density-functional theory and NiO photoemission spectra, Phys. Rev. B **48**, 16929 (1993).

[38] I. V. Solovyev, P. H. Dederichs, and V. I. Anisimov, Corrected atomic limit in the local-density approximation and the electronic structure of d impurities in Rb, Phys. Rev. B **50**, 16861 (1994).

[39] M. T. Czyżyk and G. A. Sawatzky, Local-density functional and on-site correlations: The electronic structure of La_2CuO_4 and $LaCuO_3$, Phys. Rev. B **49**, 14211 (1994).

[40] A. I. Liechtenstein, V. I. Anisimov, and J. Zaanen, Density-functional theory and strong interactions: Orbital ordering in Mott-Hubbard insulators, Phys. Rev. B **52**, R5467 (1995).

[41] V. I. Anisimov, F. Aryasetiawan, and A. I. Lichtenstein, First-principles calculations of the electronic structure and spectra of strongly correlated systems: The LDA + U method, J. Phys.: Condens. Matter **9**, 767 (1997).

[42] S. L. Dudarev, G. A. Botton, S. Y. Savrasov, C. J. Humphreys, and A. P. Sutton, Electron-energy-loss spectra and the structural stability of nickel oxide: An LSDA + U study, Phys. Rev. B **57**, 1505 (1998).

[43] A. G. Petukhov, I. I. Mazin, L. Chioncel, and A. I. Lichtenstein, Correlated metals and the LDA + U method, Phys. Rev. B **67**, 153106 (2003).

[44] M. Cococcioni and S. de Gironcoli, Linear response approach to the calculation of the effective interaction parameters in the LDA + U method, Phys. Rev. B **71**, 035105 (2005).

[45] K. P. McKenna, M. J. Wolf, A. L. Shluger, S. Lany, and A. Zunger, Two-Dimensional Polaronic Behavior in the Binary Oxides m-HfO_2 and m-ZrO_2, Phys. Rev. Lett. **108**, 116403 (2012).

[46] S. Falletta, J. Wiktor, and A. Pasquarello, Finite-size corrections of defect energy levels involving ionic polarization, Phys. Rev. B **102**, 041115(R) (2020).

[47] S. X. Zhang, D. C. Kundaliya, W. Yu, S. Dhar, S. Y. Young, L. G. Salamanca-Riba, S. B. Ogale, R. D. Vispute, and T. Venkatesan, Niobium doped TiO_2: Intrinsic transparent metallic anatase versus highly resistive rutile phase, J. Appl. Phys. **102**, 013701 (2007).

[48] R. A. Marcus, Electron transfer reactions in chemistry: theory and experiment (nobel lecture), Angew. Chem. **32**, 1111 (1993).

[49] R. A. Marcus, Chemical and electrochemical electron-transfer theory, Annu. Rev. Phys. Chem. **15**, 155 (1964).

[50] D. Emin and T. Holstein, Studies of small-polaron motion IV. Adiabatic theory of the Hall effect, Ann. Phys. **53**, 439 (1969).

[51] T. Holstein, Studies of polaron motion: Part II. The "Small" polaron, Ann. Phys. **281**, 725 (2000).

[52] I. Austin and N. Mott, Polarons in crystalline and non-crystalline materials, Adv. Phys. **18**, 41 (1969).

[53] N. A. Deskins and M. Dupuis, Electron transport via polaron hopping in bulk TiO_2: A density functional theory characterization, Phys. Rev. B **75**, 195212 (2007).

[54] H. Böttger and V. V. Bryksin, Hopping conduction in solids, in *Hopping Conduction in Solids* (Akademie-Verlag, Berlin, 1985).

[55] L. Landau, On the theory of transfer of energy at collisions II, Phys. Z. Sowjetunion **2**, 118 (1932) .

[56] C. Zener, Non-adiabatic crossing of energy levels, Proc. R. Soc. London, Ser. A **137**, 696 (1932).

[57] J. Blumberger, Recent advances in the theory and molecular simulation of biological electron transfer reactions, Chem. Rev. **115**, 11191 (2015).

[58] N. A. Deskins, R. Rousseau, and M. Dupuis, Localized electronic states from surface hydroxyls and polarons in TiO_2(110), J. Phys. Chem. C **113**, 14583 (2009).

[59] P. Liao, M. C. Toroker, and E. A. Carter, Electron transport in pure and doped hematite, Nano Lett. **11**, 1775 (2011).

[60] H. Oberhofer and J. Blumberger, Revisiting electronic couplings and incoherent hopping models for electron transport in crystalline C_{60} at ambient temperatures, Phys. Chem. Chem. Phys. **14**, 13846 (2012).

[61] J. J. Plata, A. M. Márquez, and J. F. Sanz, Electron mobility via polaron hopping in bulk ceria: A first-principles study, J. Phys. Chem. C **117**, 14502 (2013).

[62] C. Spreafico and J. VandeVondele, The nature of excess electrons in anatase and rutile from hybrid DFT and RPA, Phys. Chem. Chem. Phys. **16**, 26144 (2014).

[63] N. Adelstein, J. B. Neaton, M. Asta, and L. C. De Jonghe, Density functional theory based calculation of small-polaron mobility in hematite, Phys. Rev. B **89**, 245115 (2014).

[64] N. Alidoust and E. A. Carter, First-principles assessment of hole transport in pure and Li-doped NiO, Phys. Chem. Chem. Phys. **17**, 18098 (2015).

[65] T. J. Smart and Y. Ping, Effect of defects on the small polaron formation and transport properties of hematite from first-principles calculations, J. Phys.: Condens. Matter **29**, 394006 (2017).

[66] H. Oberhofer, K. Reuter, and J. Blumberger, Charge transport in molecular materials: An assessment of computational methods, Chem. Rev. **117**, 10319 (2017).

[67] F. Wu and Y. Ping, Combining Landau–Zener theory and kinetic Monte Carlo sampling for small polaron mobility of doped $BiVO_4$ from first-principles, J. Mater. Chem. A **6**, 20025 (2018).

[68] W. Zhang, F. Wu, J. Li, D. Yan, J. Tao, Y. Ping, and M. Liu, Unconventional relation between charge transport and photocurrent via boosting small polaron hopping for photoelectrochemical water splitting, ACS Energy Lett. **3**, 2232 (2018).

[69] T. Liu, V. Pasumarthi, C. LaPorte, Z. Feng, Q. Li, J. Yang, C. Li, and M. Dupuis, Bimodal hole transport in bulk $BiVO_4$ from computation, J. Mater. Chem. A **6**, 3714 (2018).

[70] M. Dey, A. Singh, and A. K. Singh, Formation of a small electron polaron in tantalum oxynitride: Origin of low mobility, J. Phys. Chem. C **125**, 11548 (2021).

[71] J. Tao, Q. Zhang, and T. Liu, Polaron formation and transport in Bi_2WO_6 studied by DFT + U and hybrid PBE0 functional approaches, Phys. Chem. Chem. Phys. **24**, 22918 (2022).

[72] T. Harwig and F. Kellendonk, Some observations on the photoluminescence of doped β-galliumsesquioxide, J. Solid State Chem. **24**, 255 (1978).

[73] L. Binet and D. Gourier, Origin of the blue luminescence of β-Ga_2O_3, J. Phys. Chem. Solids **59**, 1241 (1998).

[74] M. Higashiwaki, K. Sasaki, H. Murakami, Y. Kumagai, A. Koukitu, A. Kuramata, T. Masui, and S. Yamakoshi, Recent progress in Ga_2O_3 power devices, Semicond. Sci. Technol. **31**, 034001 (2016).

[75] S. J. Pearton, J. Yang, P. H. Cary, F. Ren, J. Kim, M. J. Tadjer, and M. A. Mastro, A review of Ga_2O_3 materials, processing, and devices, Appl. Phys. Rev. **5**, 011301 (2018).

[76] D. Guo, Q. Guo, Z. Chen, Z. Wu, P. Li, and W. Tang, Review of Ga_2O_3-based optoelectronic devices, Mater. Today Phys. **11**, 100157 (2019).

[77] M. J. Tadjer, J. L. Lyons, N. Nepal, J. A. Freitas, A. D. Koehler, and G. M. Foster, Editors' choice—review—theory and characterization of doping and defects in β-Ga_2O_3, ECS J. Solid State Sci. Technol. **8**, Q3187 (2019).

[78] E. G. Villora, M. Yamaga, T. Inoue, S. Yabasi, Y. Masui, T. Sugawara, and T. Fukuda, Optical spectroscopy study on β-Ga_2O_3, Jpn. J. Appl. Phys. **41**, L622 (2002).

[79] M. Yamaga, T. Ishikawa, M. Yoshida, T. Hasegawa, E. G. Villora, and K. Shimamura, Polarization of optical spectra in transparent conductive oxide β-Ga_2O_3, Phys. Status Solidi C **8**, 2621 (2011).

[80] A. M. Armstrong, M. H. Crawford, A. Jayawardena, A. Ahyi, and S. Dhar, Role of self-trapped holes in the photoconductive gain of β-gallium oxide schottky diodes, J. Appl. Phys. **119**, 103102 (2016).

[81] S. Yamaoka and M. Nakayama, Evidence for formation of self-trapped excitons in a β-Ga_2O_3 single crystal, Phys. Status Solidi C **13**, 93 (2016).

[82] B. E. Kananen, N. C. Giles, L. E. Halliburton, G. K. Foundos, K. B. Chang, and K. T. Stevens, Self-trapped holes in β-Ga_2O_3 crystals, J. Appl. Phys. **122**, 215703 (2017).

[83] Q. D. Ho, T. Frauenheim, and P. Deák, Origin of photoluminescence in β-Ga_2O_3, Phys. Rev. B **97**, 115163 (2018).

[84] A. Y. Polyakov, N. B. Smirnov, I. V. Shchemerov, S. J. Pearton, F. Ren, A. V. Chernykh, P. B. Lagov, and T. V. Kulevoy, Hole traps and persistent photocapacitance in proton irradiated β-Ga_2O_3 films doped with Si, APL Mater. **6**, 096102 (2018).

[85] T. Gake, Y. Kumagai, and F. Oba, First-principles study of self-trapped holes and acceptor impurities in Ga_2O_3 polymorphs, Phys. Rev. Mater. **3**, 044603 (2019).

[86] Y. K. Frodason, K. M. Johansen, L. Vines, and J. B. Varley, Self-trapped hole and impurity-related broad luminescence in β-Ga_2O_3, J. Appl. Phys. **127**, 075701 (2020).

[87] S. Marcinkevičius and J. S. Speck, Ultrafast dynamics of hole self-localization in β-Ga_2O_3, Appl. Phys. Lett. **116**, 132101 (2020).

[88] A. Bouzid and A. Pasquarello, Defect formation energies of interstitial C, Si, and Ge Impurities in β-Ga_2O_3, Phys. Status Solidi RRL **13**, 1800633 (2019).

[89] Y. P. Song, H. Z. Zhang, C. Lin, Y. W. Zhu, G. H. Li, F. H. Yang, and D. P. Yu, Luminescence emission originating from nitrogen doping of β-Ga_2O_3 nanowires, Phys. Rev. B **69**, 075304 (2004).

[90] J. B. Varley, J. R. Weber, A. Janotti, and C. G. Van de Walle, Oxygen vacancies and donor impurities in β-Ga_2O_3, Appl. Phys. Lett. **97**, 142106 (2010).

[91] C. Tang, J. Sun, N. Lin, Z. Jia, W. Mu, X. Tao, and X. Zhao, Electronic structure and optical property of metal-doped Ga_2O_3: A first principles study, RSC Adv. **6**, 78322 (2016).

[92] B. E. Kananen, L. E. Halliburton, K. T. Stevens, G. K. Foundos, and N. C. Giles, Gallium vacancies in β-Ga_2O_3 crystals, Appl. Phys. Lett. **110**, 202104 (2017).

[93] G. Pozina, M. Forsberg, M. Kaliteevski, and C. Hemmingsson, Emission properties of Ga_2O_3 nano-flakes: Effect of excitation density, Sci. Rep. **7**, 42132 (2017).

[94] S. Banerjee, X. Jiang, and L.-W. Wang, Designing a porous-crystalline structure of β-Ga_2O_3: A potential approach to tune its opto-electronic properties, Phys. Chem. Chem. Phys. **20**, 9471 (2018).

[95] M. E. Ingebrigtsen, J. B. Varley, A. Y. Kuznetsov, B. G. Svensson, G. Alfieri, A. Mihaila, U. Badstübner, and L. Vines, Iron and intrinsic deep level states in Ga_2O_3, Appl. Phys. Lett. **112**, 042104 (2018).

[96] H. Peelaers, J. L. Lyons, J. B. Varley, and C. G. Van de Walle, Deep acceptors and their diffusion in Ga_2O_3, APL Mater. **7**, 022519 (2019).

[97] H. J. von Bardeleben, S. Zhou, U. Gerstmann, D. Skachkov, W. R. L. Lambrecht, Q. D. Ho, and P. Deák, Proton irradiation induced defects in β-Ga_2O_3: A combined EPR and theory study, APL Mater. **7**, 022521 (2019).

[98] H. Peelaers and C. G. Van de Walle, Phonon- and charged-impurity-assisted indirect free-carrier absorption in Ga_2O_3, Phys. Rev. B **100**, 081202(R) (2019).

[99] D. Skachkov, W. R. L. Lambrecht, H. J. von Bardeleben, U. Gerstmann, Q. D. Ho, and P. Deák, Computational identification of Ga-vacancy related electron paramagnetic resonance centers in β-Ga_2O_3, J. Appl. Phys. **125**, 185701 (2019).

[100] M. D. McCluskey, Point defects in Ga_2O_3, J. Appl. Phys. **127**, 101101 (2020).

[101] J. P. Perdew, M. Ernzerhof, and K. Burke, Rationale for mixing exact exchange with density functional approximations, J. Chem. Phys. **105**, 9982 (1996).

[102] J. P. Perdew, K. Burke, and M. Ernzerhof, Generalized Gradient Approximation Made Simple, Phys. Rev. Lett. **77**, 3865 (1996).

[103] D. Wing, J. Strand, T. Durrant, A. L. Shluger, and L. Kronik, Role of long-range exact exchange in polaron charge transition levels: The case of MgO, Phys. Rev. Mater. **4**, 083808 (2020).

[104] D. Wing, G. Ohad, J. B. Haber, M. R. Filip, S. E. Gant, J. B. Neaton, and L. Kronik, Band gaps of crystalline solids from Wannier-localization-based optimal tuning of a screened range-separated hybrid functional, Proc. Natl. Acad. Sci. USA **118**, e2104556118 (2021).

[105] T. J. Smart, F. Wu, M. Govoni, and Y. Ping, Fundamental principles for calculating charged defect ionization energies in ultrathin two-dimensional materials, Phys. Rev. Mater. **2**, 124002 (2018).

[106] J. F. Janak, Proof that $\frac{\partial e}{\partial n_i} = \epsilon$ in density-functional theory, Phys. Rev. B **18**, 7165 (1978).

[107] C. Freysoldt, B. Grabowski, T. Hickel, J. Neugebauer, G. Kresse, A. Janotti, and C. G. Van de Walle, First-principles calculations for point defects in solids, Rev. Mod. Phys. **86**, 253 (2014).

[108] C. Freysoldt, J. Neugebauer, and C. G. Van de Walle, Fully *Ab Initio* Finite-Size Corrections for Charged-Defect Supercell Calculations, Phys. Rev. Lett. **102**, 016402 (2009).

[109] H.-P. Komsa, T. T. Rantala, and A. Pasquarello, Finite-size supercell correction schemes for charged defect calculations, Phys. Rev. B **86**, 045112 (2012).

[110] S. Falletta, J. Wiktor, and A. Pasquarello, Finite-size corrections of defect energy levels involving ionic polarization, https://github.com/falletta/finite-size-corrections-defect-levels (2020).

[111] S. Falletta, J. Wiktor, and A. Pasquarello, Finite-size corrections of defect energy levels involving ionic polarization, Materials Cloud Archive 2020.70 (2020), doi:10.24435/materialscloud:9p-g7.

[112] P. Giannozzi *et al.*, QUANTUM ESPRESSO: a modular and open-source software project for quantum simulations of materials, J. Phys.: Condens. Matter **21**, 395502 (2009).

[113] M. van Setten, M. Giantomassi, E. Bousquet, M. Verstraete, D. Hamann, X. Gonze, and G.-M. Rignanese, The PseudoDojo: Training and grading a 85 element optimized norm-conserving pseudopotential table, Comput. Phys. Commun. **226**, 39 (2018).

[114] P. Umari and A. Pasquarello, *Ab initio* Molecular Dynamics in a Finite Homogeneous Electric Field, Phys. Rev. Lett. **89**, 157602 (2002).

[115] A. Alkauskas and A. Pasquarello, Band-edge problem in the theoretical determination of defect energy levels: The O vacancy in ZnO as a benchmark case, Phys. Rev. B **84**, 125206 (2011).

[116] M. Passlack, E. F. Schubert, W. S. Hobson, M. Hong, N. Moriya, S. N. G. Chu, K. Konstadinidis, J. P. Mannaerts, M. L. Schnoes, and G. J. Zydzik, Ga_2O_3 films for electronic and optoelectronic applications, J. Appl. Phys. **77**, 686 (1995).

[117] H. H. Tippins, Optical absorption and photoconductivity in the band edge of β-Ga_2O_3, Phys. Rev. **140**, A316 (1965).

[118] R. C. Weast, M. Astle, and W. Beyer, *CRC Handbook of Chemistry and Physics* (CRC Press, Boca Raton, FL, 1985).

[119] C. G. Van de Walle and P. E. Blöchl, First-principles calculations of hyperfine parameters, Phys. Rev. B **47**, 4244 (1993).

[120] F. Mauri, B. G. Pfrommer, and S. G. Louie, *Ab Initio* Theory of NMR Chemical Shifts in Solids and Liquids, Phys. Rev. Lett. **77**, 5300 (1996).

[121] N. Varini, D. Ceresoli, L. Martin-Samos, I. Girotto, and C. Cavazzoni, Enhancement of DFT-calculations at petascale: Nuclear magnetic resonance, hybrid density functional theory and Car–Parrinello calculations, Comput. Phys. Commun. **184**, 1827 (2013).

[122] H. Jónsson, G. Mills, and K. W. Jacobsen, Nudged elastic band method for finding minimum energy paths of transitions, in *Classical and Quantum Dynamics in Condensed Phase Simulations* (World Scientific, Singapore, 1998), pp. 385–404.

[123] A. Alkauskas, J. L. Lyons, D. Steiauf, and C. G. Van de Walle, First-Principles Calculations of Luminescence Spectrum Line Shapes for Defects in Semiconductors: The Example of GaN and ZnO, Phys. Rev. Lett. **109**, 267401 (2012).

[124] A. Alkauskas, Q. Yan, and C. G. Van de Walle, First-principles theory of nonradiative carrier capture via multiphonon emission, Phys. Rev. B **90**, 075202 (2014).

[125] Z. Wang and K. H. Bevan, Exploring the impact of semicore level electronic relaxation on polaron dynamics: An adiabatic *ab initio* study of $FePO_4$, Phys. Rev. B **93**, 024303 (2016).

[126] R. P. Bell and C. N. Hinshelwood, The theory of reactions involving proton transfers, Proc. R. Soc. London A **154**, 414 (1936).

[127] M. G. Evans and M. Polanyi, Inertia and driving force of chemical reactions, Trans. Faraday Soc. **34**, 11 (1938).

[128] S. Falletta and A. Pasquarello, Materials Cloud Archive 2023.70 (2023), doi:10.24435/materialscloud:fy-86.